J Solid State Electrochem (2012) 16:1111–1119
DOI 10.1007/s10008-011-1504-7

ORIGINAL PAPER

TiO_2/WO_3 photoanodes with enhanced photocatalytic activity for air treatment in a polymer electrolyte cell

Jenia Georgieva

Received: 18 April 2011 / Revised: 4 July 2011 / Accepted: 5 July 2011 / Published online: 22 July 2011

Abstract The application of electrochemically enhanced photocatalysis in air treatment using a Nafion-based photoelectrochemical cell and TiO_2/WO_3 photoanodes for organic vapor photooxidation under both UV and visible light irradiation is briefly presented. In that direction, the obtained results regarding the preparation and characterization of the TiO_2/WO_3 photoanodes with enhanced photocatalytic activity are reviewed. Particular emphasis is given in the comparison of the photocatalytic behavior of bilayer TiO_2/WO_3 coatings, electrosynthesized on stainless steel mesh and powder C + mixed (WO_3 + TiO_2) photoanodes. The advantages of using a high surface area C + mixed (WO_3 + TiO_2) powder catalysts as photoanodes against their plain TiO_2 + C and WO_3 + C analogues are discussed.

Keywords TiO_2/WO_3 photoanodes · Air treatment · Polymer electrolyte cell · Photooxidation

Introduction

One of the attractive technologies for water and air treatment is that of heterogeneous photocatalysis, which can lead to rapid and efficient degradation of a wide range of common organic pollutants [1–4]. Its application allows the oxidation of gas-phase volatile organic contaminants (VOCs) [5] to CO_2 and H_2O at room temperature with the help of a semiconductor catalyst and a UV or near-UV light source.

J. Georgieva (✉)
Rostislaw Kaischew Institute of Physical Chemistry,
Bulgarian Academy of Sciences,
1113 Sofia, Bulgaria
e-mail: jenia@ipc.bas.bg

In photocatalytic air and water purification processes, dissolved or VOCs are destroyed by oxidation in the presence of photoactive semiconductor catalysts utilizing artificial or solar UVA and visible light irradiation. The catalyst can either be in the form of a slurry suspension or supported on solid substrates. When the semiconductor photocatalyst is illuminated with photons possessing energies greater than the band gap of the catalyst in the presence of water and oxygen, the absorbed photons then excite valence electrons into the conduction band, creating positive holes. The photogenerated holes at the valence band react with water and produce highly reactive and powerful hydroxyl radicals ($OH^{\cdot}$) that attack the organics, while the photogenerated electrons at the conduction band react with oxygen and produce superoxide radicals (Fig. 1a). In some cases, there is also direct scavenging of holes by the organic species itself resulting in its direct photooxidation. When the photocatalyst is immobilized on an electronic conductor, the application of an external positive bias in an appropriate cell can draw the photogenerated electrons away from the catalyst surface through the external cell circuit while photogenerated holes are being transferred to the electrode surface (Fig. 1b). In this way, the rate of electron–hole recombination is decreased and the rate of surface reactions increased. This process is known as electrically enhanced photocatalysis or photoelectrocatalysis [6–11].

One of the most popular photocatalysts is TiO_2, a wide gap n-type semiconductor [12] for the oxidation of gaseous or aqueous organic pollutants because of its excellent chemical stability and good catalytic activity towards the photooxidation of organic compounds. It is also commercially available and inexpensive. However, TiO_2 photocatalysts absorb only UV light and thus it would be desirable for practical applications to develop photocata-

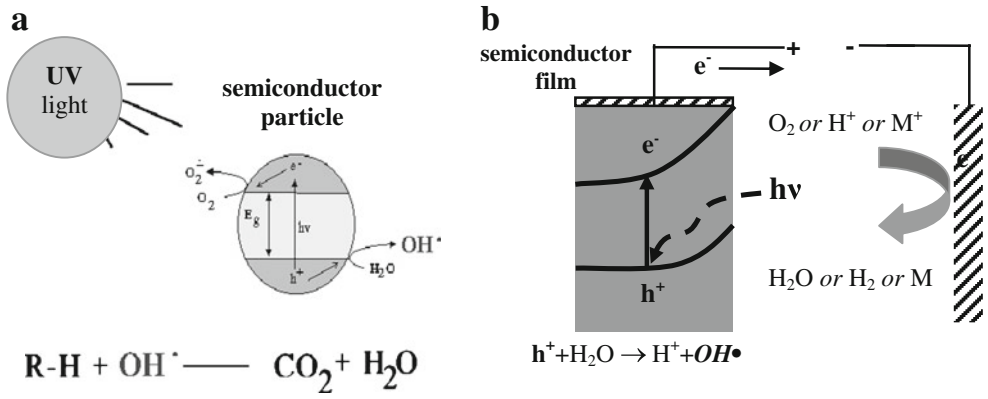

Fig. 1 Principle of photocatalytic (**a**) and photoelectrocatalytic (**b**) treatment of organics

lysts which exhibit visible light response too, aiming at the utilization of solar radiation. Coupling TiO_2 with WO_3 (a semiconductor of a smaller bandgap which is active under visible light [13–15]) is a strategy for achieving two main targets: reducing photogenerated electron–hole recombination rates (by synergism at the heterojunction due to valence and conduction band energies mismatch) [16] and expanding their useful range of operation into visible spectral region. In more details, as shown by the valence and conduction band energy diagrams of the two materials, electron injection is favored from the conduction band of TiO_2 to that of WO_3 and hole transfer between valence bands in the opposite direction, during UV illumination (Fig. 2a). This in turn reduces electron–hole recombination in both semiconductors. During visible (Vis) light illumination, photogenerated electrons and holes are only created in WO_3 but the latter still move to the TiO_2 valence band under the influence of the electric field within TiO_2 (Fig. 2b).

Electrosynthesis of TiO_2 and electrodeposition of WO_3 have been proposed as an alternative route for the preparation of plain or mixed coatings on conducting substrates because of some advantages of the electrochemical methods like simplicity of equipment and accurate control of coating thickness. Electrochemically obtained

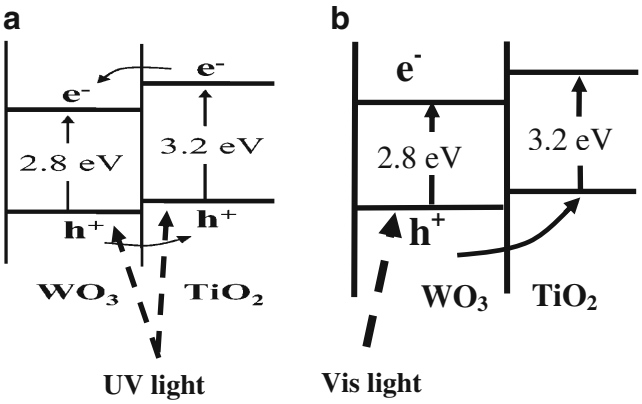

Fig. 2 Principle of TiO_2–WO_3 photocatalytic synergism under UV light (**a**) and Vis light (**b**)

semiconductors can be used as photoanodes [17–30]. Although mixed TiO_2/WO_3 photoanodes have been successfully tested for water treatment, there is no report of their performance in gas-phase photoelectrocatalysis. Besides, the data in the literature about the photooxidation of organics in the gas phase using all-solid photoelectrochemical cells are very scarce. Enea [31] first proposes a porous cell for photo-assisted electrooxidations in the gas phase. This cell is based on a liquid electrolyte, making its incorporation into a gas-phase photoreactor impractical. Solid polymer or gel electrolyte systems are usually employed in dye-sensitized solar cells (DSSCs) [32, 33]. There are very few articles on Nafion-supported TiO_2 photoanodes focused on CO_2 reduction and hydrogen production. Ichikawa and Doi [34] use an all-solid photoelectrochemical cell of a non-DSSC type, employing a Nafion® membrane as the polymer electrolyte for the production of hydrogen by water photooxidation at the anode and the reduction of CO_2 at the cathode. A polymer membrane electrode assembly consisting of a TiO_2 photoanode, a Pt cathode, and a proton exchange membrane (Nafion) was constructed to generate hydrogen continuously under UV excitation with no applied bias [35]. Since the used photoanodes consisted of plain TiO_2, no visible light activity was observed.

We have recently introduced the first all-solid Nafion-based photoelectrochemical cell for organic vapor photooxidation under both UV and visible light irradiation as a proof of concept for the application of electrochemically enhanced photocatalysis in air treatment [36–38]. The concept of a polymer electrolyte photoelectrochemical cell is presented in Fig. 3.

Bilayer TiO_2/WO_3 coatings, electrosynthesized on stainless steel mesh [36] and more practical powder catalysts C + TiO_2 [37], C + WO_3, and C + mixed WO_3/TiO_2 [38] have been tested as photoanodes. It was very important to check the possibility to use as a photoanode C + mixed WO_3/TiO_2 powder catalysts instead of electrosynthesized bilayer TiO_2/WO_3 coatings on stainless steel. The powder catalysts combine the advantage of a bifunctional material [active both

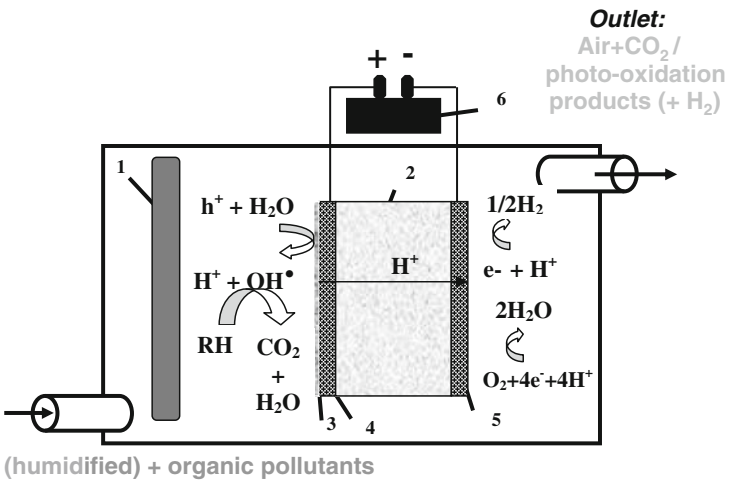

Fig. 3 Concept of a polymer electrolyte photoelectrochemical cell: *1* lamp, *2* solid polymer electrolyte membrane, *3* porous TiO_2-based anode, *4* stainless steel mesh or porous electrode layer, *5* stainless steel mesh cathode, *6* power supply

under UV and Vis light] with those of high surface area and simplicity of preparation. Besides the larger catalytic surface of powder coatings, the replacement of a stainless steel support by carbon offers the opportunity to expand the applied potential range of photoelectrochemical experiments to higher values at no substrate anodic dissolution risk.

The aim of this paper is to summarize the obtained results in our laboratories regarding TiO_2/WO_3 photoanodes for air treatment. These include the preparation of the photoanodes, their microscopic and photoelectrochemical characterization. The specific objectives are (1) to compare the photoelectrocatalytic activity of electrosynthesized bilayer TiO_2/WO_3/stainless steel (SS) coatings and powder photoanodes, in the presence of water and methanol vapors, under UV and visible light irradiation, and (2) the optimization of the powder photoelectrodes' composition in terms of their enhanced photocatalytic activity under both UV and Vis light illumination.

Electrosynthesized bilayer TiO_2/WO_3 coatings on stainless steel substrates

Preparation of TiO_2/WO_3/SS photoanodes

Stainless steel square substrates (3×3 cm) were cut from an AISI 304 (Fe/Cr18/Ni10) plain weave mesh of 40×40 wires per inch, with a wire diameter of 250 μm and a 37% open area (Goodfellow), degreased ultrasonically with acetone and etched in a 1/1 HCl/H_2O mixture for 60 s before the electrochemical preparation of the coatings. For electrodeposition/electrosynthesis we employed an Autolab 30 potentiostat (EcoChemie) with a 20 A booster and a 2-L three-electrode cell using SS substrate as a cathode, platinized titanium plates as counter electrodes, and mercurous sulfate $Hg/Hg_2SO_4/H_2SO_4$ (0.5 M) electrode (MSE) as a reference electrode.

WO_3 was obtained from a bath of pH=1.4 containing 0.025 M Na_2WO_4 ($Na_2WO_4{\cdot}2H_2O$, Merck, pro analysi, >99%), 0.03 M H_2O_2 (30% aqueous solution), and 0.05 M HNO_3 (Riedel, 65%) by potentiostatic cathodic deposition for 30 min at −1.00 V vs. MSE. The electrodeposited film was heated at 350 °C for 30 min for crystallization (monoclinic WO_3, as confirmed by XRD [30]). TiO_2 layer was electrosynthesized on top of the already formed WO_3 layer by keeping the WO_3/SS electrode at −2.00 V vs. MSE from a solution of pH=1.4 containing 0.02 M $TiOSO_4$ (Fluka; Assay of Ti (as TiO_2) techn., >29%), 0.03 M H_2O_2 (30% aqueous solution), 0.05 M HNO_3 (Riedel, 65%), and 0.1 M KNO_3 (Merck, pro analysi, >99%) [15, 17, 18, 20–30, 36]. After electrosynthesis, the deposited gel film was heated in air at 400 °C for 1 h to obtain crystalline TiO_2 (anatase, as confirmed by XRD [30]) film. Typical WO_3 and TiO_2 loadings (per true substrate geometric area) were 0.8–1.0 mg cm^{-2} and 0.2–0.4 mg cm^{-2}, respectively.

Microscopic characterization of catalysts

Scanning electron microscopy (SEM) was carried out using a JEOL JSM 6390 microscope equipped with an EDS facility. Figure 4 shows SEM images of a TiO_2/WO_3 bilayer coating (0.40 mg cm^{-2} TiO_2/0.86 mg cm^{-2} WO_3 loading) on a stainless steel mesh. The coating consists of flakes that are uniformly distributed over the wires' surface (Fig. 4a). A “cracked mud” morphology is observed, characterized by 5–30 μm large patches or islands further decorated by smaller aggregates of nanoparticles and separated by cracks (Fig. 4b). There is extensive mixing of WO_3 and TiO_2 (necessary for successful synergism), and TiO_2 pertains on island surfaces whereas WO_3 within the cracks, in accordance with Auger electron and Raman spectroscopy experiments presented in [24, 29]. This open structure, where both components are exposed to light and the solution or vapors, is a prerequisite to a good photocurrent

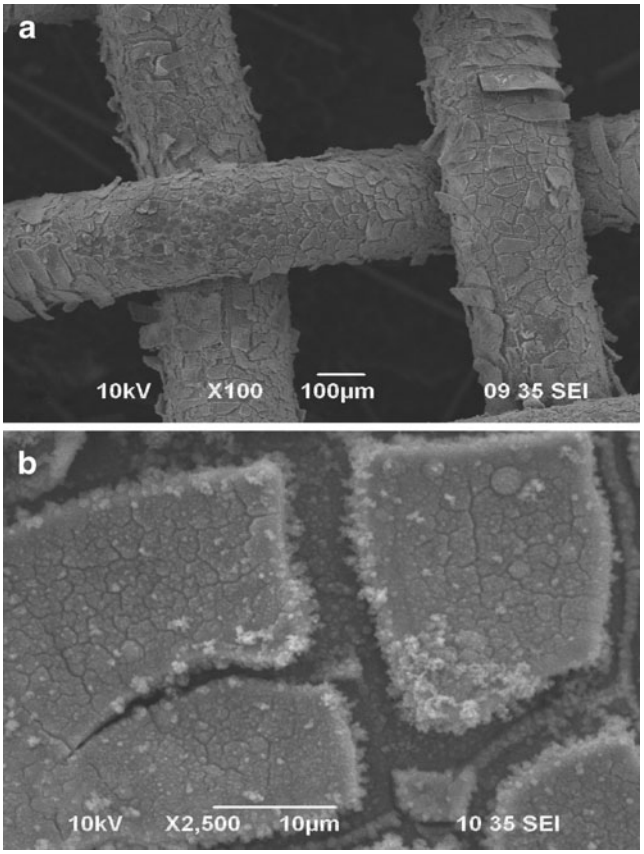

Fig. 4 SEM images of bilayer TiO_2/WO_3 coating on SS mesh after annealing for 1 h at 400 °C at two different magnifications (**a**, **b**)

response under both UV and visible light illumination via synergy.

Powder TiO_2/WO_3/C photoanodes

Preparation of powder TiO_2/WO_3/C photoanodes

Powder catalysts C + WO_3, C + TiO_2, and C + mixed (WO_3 + TiO_2) powders were prepared by mixing the appropriate quantities of TiO_2 (Degussa® P-25), WO_3 powder (Fluka), and C (carbon black) dispersed in ethanol. The mixtures were mechanically grinded in a mortar and then dried at 200 °C for 2 h. Different samples [C + mixed (WO_3 + TiO_2)] were prepared, varying the atomic ratio W to Ti (from 1.0:2.0 to 2.0:1.0), as well as the weight ratio of the photocatalyst (WO_3 + TiO_2) and C (from 1:1 to 5:1). The photocatalyst loading has been in the 0.40–0.45 mg range [38].

Microscopic characterization of catalysts

SEM was performed using a JEOL JSM 6390 SEM to give the morphology and agglomerated particle size. Backscattered electron images (BEI) and secondary electron images (SEI) of the obtained C + mixed (WO_3 + TiO_2) (0.225 mg C, 0.27 mg WO_3, 0.18 mg TiO_2), C + WO_3 (0.20 mg C, 0.40 mg WO_3), and C + TiO_2 (0.20 mg C, 0.40 mg TiO_2) catalysts are shown in Fig. 5a–c. On the top of the catalyst layers, one can see particles and agglomerates of particles of different size, distributed within the carbon powder support. This inhomogeneity is due to the agglomeration of nanometer-sized particles (20–30 nm for TiO_2 and 60 nm for WO_3 as confirmed by XRD analysis) resulting from catalyst grinding, thermal treatment, and mixing with the Nafion® binder. In the backscattered (BEI)

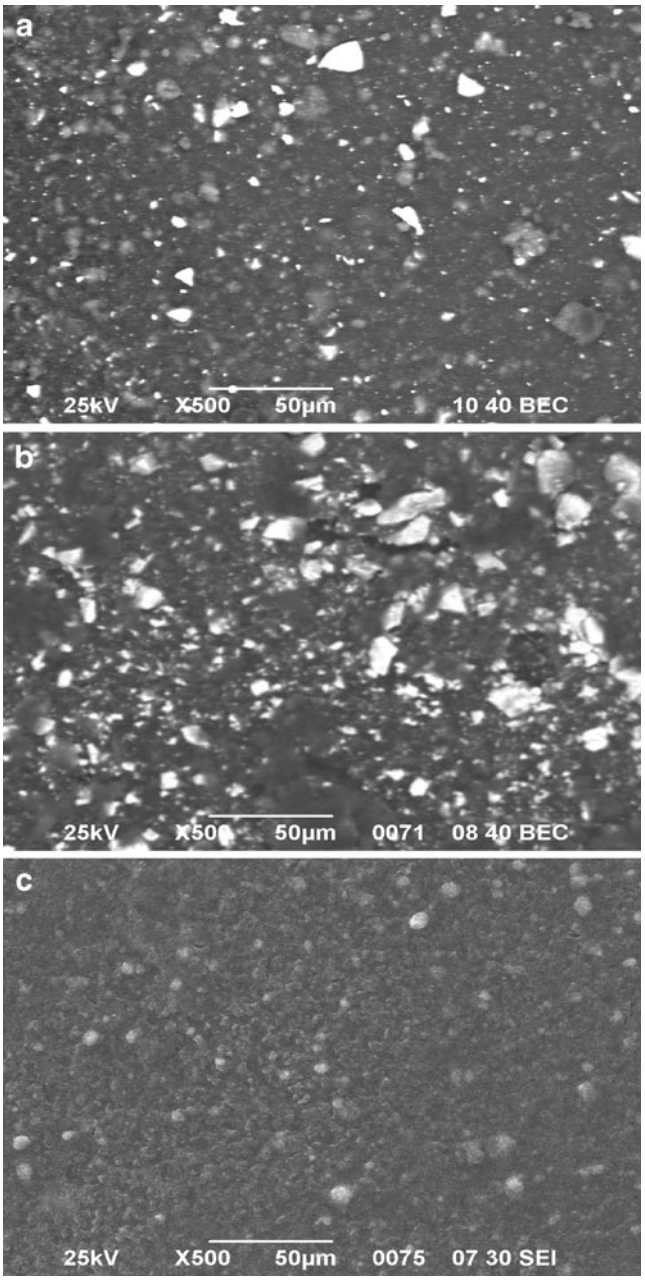

Fig. 5 SEM images (BEI) of C + mixed WO_3/TiO_2 (**a**), C + WO_3 (**b**), and (SEI) of C+TiO_2 (**c**)

SEM images (Fig. 5a, b), bright areas correspond to WO_3, grey areas in Fig. 5 to TiO_2, and dark areas in Fig. 5a, b to carbon. This chemical contrast is due to the higher yield of electrons, backscattered by the element with a greater atomic mass (W). In terms of the morphology, the SEI of the C + TiO_2 powder catalyst (Fig. 5c) is more informative than BEI due to the lack of clear chemical contrast between Ti and carbon. A comparison between Fig. 5a–c also shows the greater tendency of WO_3 particles to agglomeration.

Fabrication of the solid polymer electrolyte photoelectrochemical cell and photoelectrochemical setup

A schematic diagram of the solid polymer electrolyte photoelectrochemical cell is presented in Fig. 6. A HT Tuffryn polysulfone membrane (2.5 cm disc) with 0.45 μm pore size (Gelman Sciences) was used as an electrode separator and support of the solid polymer electrolyte. The membrane was impregnated with a Nafion® (Aldrich, protonic form), 5% *w/w* solution in a mixture of low aliphatic alcohols and 45% water and then left to dry in ambient air overnight. A rectangular specimen of TiO_2/WO_3/SS mesh was adhered on one face of the membrane with the help of a few drops of the Nafion® solution [36]. The total mesh area in contact with the electrolyte was 1.6 cm^2 (true SS wire geometric areas of 4.0 cm^2). Powder catalysts were made into photoelectrode layers by mixing with the proton conductor of Nafion® and pasting onto the porous membranes [37, 38]. Then they were left to dry for 30 min in air. The working area of the powder samples was 0.3 cm^2. The photoelectrochemical mini-cell was completed by adhering an Ag/AgCl wire reference electrode and a larger (2×2 cm) piece of plain SS mesh cathode on the same and opposite sides of the membrane respectively.

The photocatalysts were tested for their photoelectrocatalytic activity in the presence of pure water vapor and in the presence of the model volatile organic of methanol. The test reactor was a 500-ml cylindrical cell with a removable cap. A Radium Ralutec 9W/78 UVA lamp (λ=350–400 nm, λ_{max}= 369 nm) or a Radium Ralutec 9W/71 visible light lamp (λ> 400 nm, λ_{max}=437 nm) placed in a cylindrical sleeve was introduced from an opening in the middle of the cap leaving an available volume of 300 ml. The power density at the electrode surface was measured as 3 mW cm^{-2} with a photometer. The photoelectrochemical cell was taped onto the external wall of the lamp sleeve with the photoelectrode facing the lamp. Plastic tubing was inserted into the reactor from openings at the top to serve as the gas inlet and outlet. The test gas was air, saturated with the vapors of MeOH/H_2O solutions after passing (via a small pump) through a Dreshler flask containing 200 ml of the appropriate methanol–water solution. Methanol aqueous solutions 1–10% *w/w* were used to achieve methanol vapor partial pressures in the 1.2–13.5-Torr range, as estimated from saturated methanol vapor pressure *x–y–T* data [39]. Cyclic voltammetry and photoamperometry at the three-electrode cell were carried out with the Autolab 100 (EcoChemie) system.

Gas-phase photoelectrochemistry of electrosynthesized TiO_2/WO_3/SS photoanodes

Figure 7a, b presents results of constant potential (+0.5 V vs. Ag/AgCl) photoamperometric experiments at a TiO_2

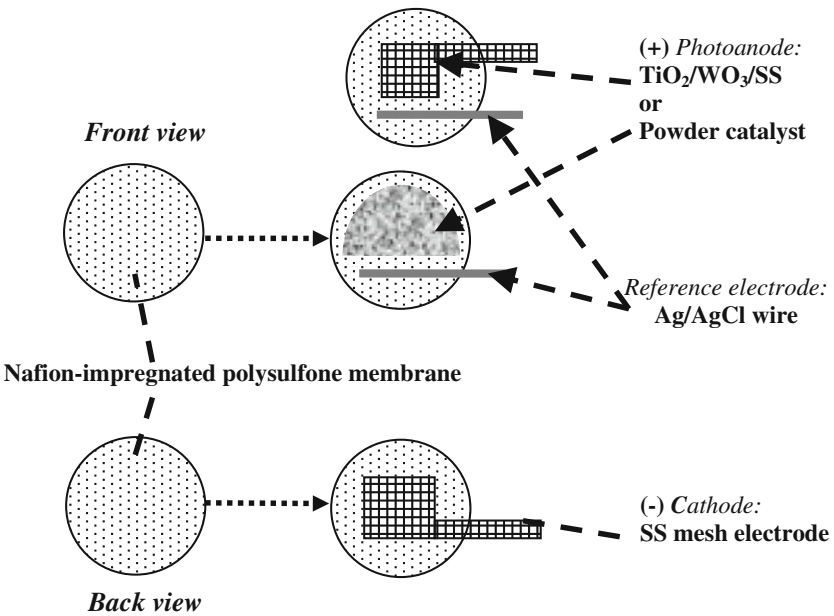

Fig. 6 Schematic representation of the all-solid photoelectrochemical cell

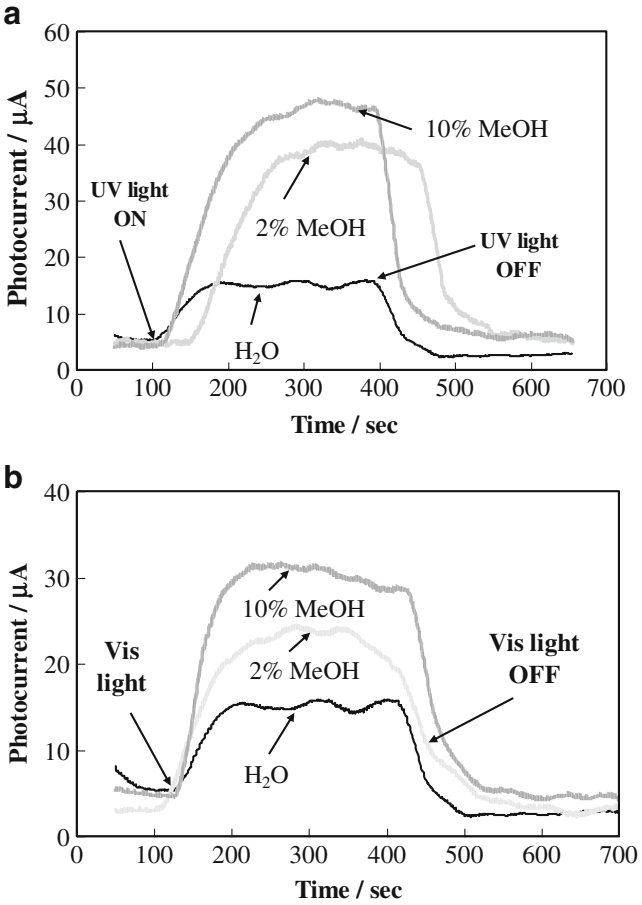

Fig. 7 Photoamperometric curves of the TiO_2/WO_3/SS photoelectrode, biased at +0.5 V vs. Ag/AgCl, in water-saturated 2% and 10% MeOH-saturated air streams, under UV (**a**) and Vis light (**b**) irradiation

(0.40 mg cm^{-2})/WO_3 (0.86 mg cm^{-2})/SS photoelectrode under UV light (Fig. 7a) or visible light (Fig. 7b) in air streams saturated either with pure water vapor or with the vapors of 2% and 10% *w*/*w* MeOH aqueous solutions [36]. It can be seen that in the presence of methanol, the photocurrent, I_{ph}, is higher, indicating that methanol scavenges photogenerated holes [40] at the electrode surface or/and adsorbed $OH^{\cdot}$ radicals [41] rather than $OH^{\cdot}$ reacts with methanol dissolved in the polymer electrolyte. The significant enhancement of visible photoactivity of bilayer sample is at a first glance unexpected since the TiO_2 overlayer cannot be activated on its own to a significant extent by visible light illumination. Efficient visible light absorbance by WO_3 can then only be considered if either the TiO_2 overlayer is thin enough to be transparent to visible light or microporous (at least at locations). In a recent series of papers [24, 27–30], we have demonstrated that, in aqueous solutions, WO_3 improves the UV photocatalytic activity of TiO_2. This effect has been attributed to electron injection from the conduction band of TiO_2 to that of WO_3 and hole transfer between valence bands in the opposite direction which in turn reduces electron–hole recombination in both semiconductors [16]. On the other hand, TiO_2 increases the visible light activity of WO_3. This effect can be explained in the following way. The photogenerated holes from the valence band of WO_3 are transferred to the valence band of TiO_2. There they would move to the surface under the influence of the electric field caused by the excess positive charge of the n-type TiO_2 semiconductor in contact with an electrolyte solution (which becomes negatively charged) and the resulting band bending (which is even more pronounced under no excitation of TiO_2 under visible light). The holes oxidize water to $OH\cdot$ at the electrode surface, thus creating active catalytic sites [42]. In this way both semiconductors are involved in the photocatalytic oxidation process. Because photocarriers in WO_3 are constantly excited by visible light, the hole flux toward TiO_2 is available as long as the rate of the carriers' recombination is effectively decreased.

The role of the positive bias potential and the good electronic contact with SS should be even greater with respect to UV light. The successful work of this mechanism also depends on the good intermixing of the two semiconductors and the free access of both light and treated solution [29].

Under UV illumination, a plot of C_{MeOH}/I_{ph} vs. C_{MeOH} was found linear in the 1–10% *w*/*w* range [36] indicating that photooxidation at both TiO_2 and WO_3 obeys the formalism of the Langmuir–Hinselwood kinetics equation [43]. Such a correlation could not be made in the case of visible light irradiation, since TiO_2 is not visibly active itself and its beneficial effect on catalytic activity appears to be more complicated, as discussed above.

Photoelectrochemical characterization of powder TiO_2/WO_3/C photoanodes in gas phase

Photovoltammetric and photoamperometric experiments in a gas stream saturated with water vapor or with the vapors of a 5% *w*/*w* MeOH aqueous solution, under UV and Vis light illumination, have been performed [38]. Three different samples were tested having a W to Ti atomic composition ratio of 1.2:1, 1:2, and 2:1 respectively in order to optimize the composition of the powder photoelectrodes. The catalyst to carbon, (TiO_2 + WO_3) to C, weight ratio of all three tested photocatalysts was 2:1. Performing preliminary experiments, this weight ratio of (WO_3 + TiO_2) catalyst and C was identified as appropriate for the system. When the carbon quantity is too much (catalyst to C weight ratio, 1:1), the light can not penetrate effectively through the mixture to reach and excite most of the photocatalyst. On the other hand, very small carbon loadings (catalyst to C weight ratio, 5:1) do not provide

sufficient electronic conductivity to the system. We can summarize the obtained results as follows: (1) the obtained photocurrents are higher than the ones observed at TiO_2/WO_3/SS meshes [36], as expected for the much higher surface area of the powder electrodes; (2) overall, the powder catalyst are active both under Vis and UV illumination as expected for their binary nature and the fact that TiO_2 is active under UV light whereas WO_3 under both UV and Vis light; and (3) the photocurrent rises in the presence of the organic vapor of MeOH, indicating its direct photooxidation via uptake of photogenerated holes.

The catalyst having an atomic composition ratio of 1W to 2Ti was selected for the next experiments, bearing in mind its considerable photoelectrocatalytic activity under both UV and Vis light irradiation [38]. Figure 8a, b presents the results of constant potential (+1.0 V vs. Ag/AgCl) photoamperometric experiments under UV or Vis light illumination in air streams saturated either with pure water vapor or with the vapors of MeOH aqueous solutions of varied methanol concentration. The behavior of the powder photoelectrodes is similar to that of TiO_2/WO_3/SS electrodes. A clear photocurrent increase can be seen with increasing methanol concentration up to 5% *w*/*w* MeOH, indicating that methanol scavenges photogenerated holes or/and adsorbed $OH^{\cdot}$ radicals at the electrode surface.

In our previous studies [24, 27–30], it was found that the application of an external bias and the use of electro-synthesized bilayer TiO_2/WO_3 on a stainless steel substrate both improve the photelectrocatalytic activity with respect to those observed at plain TiO_2 coatings under UV and at plain WO_3 coatings under both UV and visible light illumination. In that direction the photoelectrocatalytic activity of C + mixed (WO_3 + TiO_2) catalyst was compared with that of C + WO_3 and C + TiO_2 photoelectrodes (of similar total photocatalyst load of 0.45–0.40 mg) with respect to the photooxidation of water (Fig. 9a) and methanol vapors (Fig. 9b), under both UV and visible light activation [38].

Under UV light irradiation, the photocurrent at the C + mixed (WO_3 + TiO_2) is equal or higher to that of its plain C + TiO_2 and C + WO_3 components both in water-

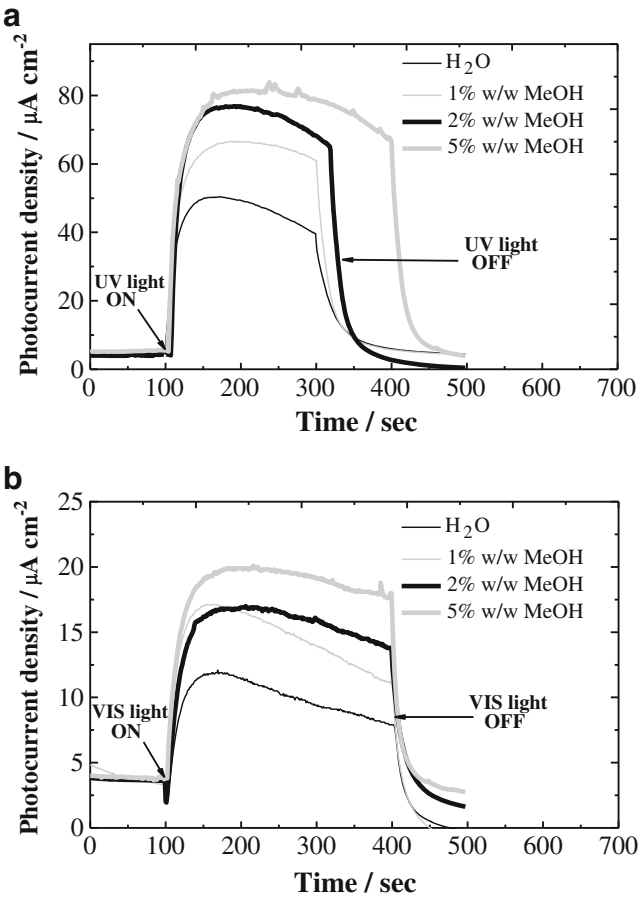

Fig. 8 Photoamperometric curves at (TiO_2 + WO_3 + C)/Nafion® photoelectrode of the all-solid cell, biased at +1.0 V vs. Ag/AgCl, in water-saturated and 1%, 2%, and 5% *w*/*w* MeOH-saturated air streams, under UV (**a**) and Vis light (**b**) illumination

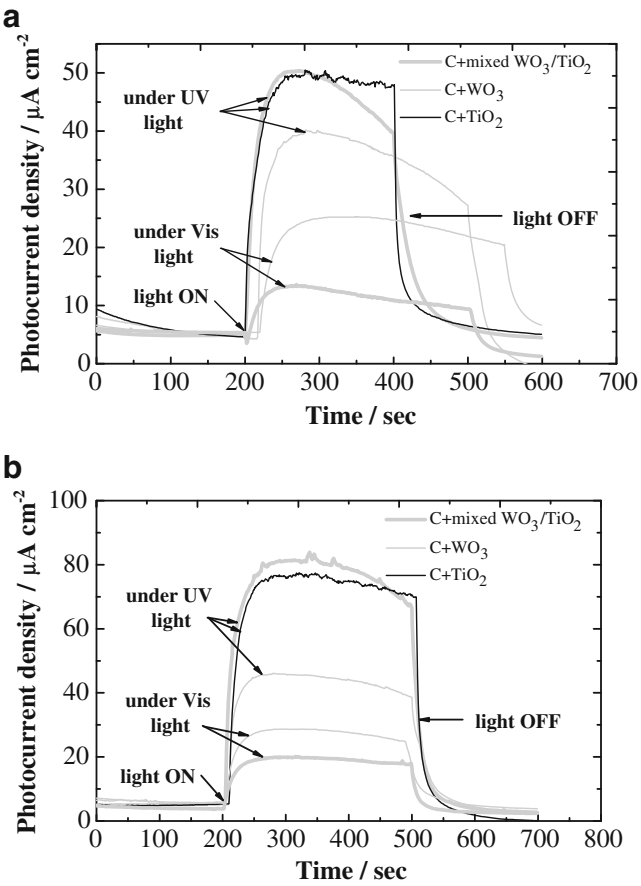

Fig. 9 Photoamperometric curves at C + mixed (WO_3 + TiO_2), C + WO_3, and C + TiO_2 photoelectrodes of the all-solid cell, biased at +1.0 V vs. Ag/AgCl, in water-saturated (**a**) and in 5% *w*/*w* MeOH-saturated air streams (**b**), under Vis and UV light illumination

saturated and MeOH-saturated vapors. It has to be underlined that the quantity of the TiO_2 photoactive material present in the C + mixed (WO_3 + TiO_2) catalyst is almost half that of the plain one and the quantity of WO_3 is also lower in the mixture than in the plain catalyst. This means that there is synergism between the two photoactivate components, which is in accordance with the extensive synergism observed at electrosynthesized bilayer WO_3/TiO_2 coatings, implying that mixing mechanically WO_3 and TiO_2 can also provide good and/or high surface area electronic contact between the two semiconductors. The latter is very important for photocatalytic activity improvement via hole and electron transfer between the two components, as mentioned above. The lowest photocurrent is observed at the plain WO_3.

Under visible light irradiation, the photocurrent at the C + WO_3 catalyst is higher than that at the C + mixed (WO_3 + TiO_2) anode especially in the case of water (Fig. 9a) but it is suppressed in the presence of MeOH (Fig. 9b). In contrast to electrosynthesized TiO_2/WO_3 bilayer coatings [24, 27–30, 36], where TiO_2 overlayer is very thin and/or porous, permitting visible light activation of the entire surface, in the mixed anodes, the lower quantity of WO_3 whose exposed surface is further reduced by mixing replacing it with Vis light inactive TiO_2 cannot be offset by a visible light synergism between WO_3 and TiO_2. In the C + mixed (WO_3 + TiO_2) coatings, visible light synergism can only occur at the interface between the topmost TiO_2 and WO_3 particles with large TiO_2 particles not being activated by visible light and not allowing either its penetration to reach and photoactivate WO_3 particles that lie underneath.

Comparing Fig. 9a, b one may notice that the shapes of the photocurrent transients in water (Fig. 9a) and methanol (Fig. 9b) differ. In the presence of methanol, the shapes are squarer compared with these in water media, which is indicating a minor degree of recombination (scavenging of holes by methanol molecules). Also, the effect of MeOH on the photocurrent at the C + WO_3 catalyst is insignificant under both UV and visible light illumination. This fact indicates the preferential water photooxidation to $OH^{\cdot}$ at WO_3; these may further react to produce oxygen or oxidize dissolved methanol. The addition of TiO_2 results in a photocurrent increase in the presence of methanol, presumably due to direct methanol oxidation at TiO_2 sites under UV illumination or under Vis illumination. This is a potential advantage of using a TiO_2 + WO_3 electrode of this kind (instead of a plain WO_3 one) for the destruction of organics under Vis light.

Conclusions

1. The possibility of using bilayer TiO_2/WO_3 coating electrosynthesized on stainless steel or C + mixed (WO_3 + TiO_2) powder catalyst as a photoanode in an all-solid photoelectrochemical cell with a polymer electrolyte for air treatment has been presented.
2. The tested TiO_2/WO_3 photoanodes are active under both UV and visible light illumination, making them applicable to artificial and sunlight irradiation applications.
3. Besides the simplicity of preparation, the powder catalysts show better photoactivity than electrosynthesized bilayer TiO_2/WO_3/SS coatings due to their larger surface area. On the other hand, electrosynthesized bilayer TiO_2/WO_3 coatings can be excited more effectively by visible light due to the good electronic contact with SS substrate and extensive mixing of WO_3 and TiO_2 (necessary for successful synergism).
4. The composition of the powder photoelectrodes has been optimized in terms of their enhanced photocatalytic activity under both UV and Vis light irradiation.
5. Under UV light irradiation, the photocurrents obtained at C + mixed (WO_3 + TiO_2) anodes are higher than those on plain TiO_2 + C and WO_3 + C analogues both in water-saturated and MeOH-saturated vapors due to synergism between the two photoactivated components. The direct methanol photooxidation under both UV and Vis light irradiation is another advantage of using a C + mixed (WO_3 + TiO_2) electrode for the destruction of organics.

References

1. Hoffmann MR, Martin ST, Choi W, Bahnemann DW (1995) Chem Rev 95:69–96
2. Mills A, Le Hunte V (1997) J Photochem Photobiol Chem 108:1–35
3. Fujishima A, Rao TN, Tryk DA (2000) J Photochem Photobiol C Photochem Rev 1:1–21
4. Rajeshwar K, Osugi ME, Chanmanee W, Chenthamarakshan CR, Zanoni MVB, Kajitvichyanukul P, Krishnan-Ayer R (2008) J Photochem Photobiol C Photochem Rev 9:171–192
5. Dibble LA, Raupp GB (1990) Catal Lett 4:345–354
6. Butterfield IM, Christensen PA, Hamnett A, Shaw KE, Walker GM, Walker SA, Howarth CR (1997) J Appl Electrochem 27:385–395
7. Candal RJ, Zeltner WA, Anderson MA (1999) J Environ Eng 125:906–912
8. Fernandez-Ibanez P, Malato S, Enea O (1999) Catal Today 54:329–339
9. Christensen PA, Curtis TP, Egerton TA, Kosa SAM, Tinlin JR (2003) Appl Catal B Environ 41:371–386
10. Egerton TA, Christensen PA, Kosa SAM, Onoka B, Harper JC, Tinlin JR (2006) Int J Environ Pollut 27:2–19
11. Fraga LE, Anderson MA, Beatriz MLPMA, Paschoal FMM, Romão LP, Zanoni MVB (2009) Electrochim Acta 54:2069–2076
12. Finklea HO (ed) (1998) Semiconductor electrodes. Elsevier, Amsterdam, pp 43–145
13. Ohno T, Tanigawa F, Fujihara K, Izumi S, Matsumura M (1998) J Photochem Photobiol Chem 118:41–44
14. Santato C, Ulmann M, Augustynski J (2001) J Phys Chem B 105:936–940

15. Luo J, Hepel M (2001) Electrochim Acta 46:2913–2922
16. Miyauchi M, Nakajima A, Watanabe T, Hashimoto K (2002) Chem Mater 14:4714–4720
17. Natarajan C, Nogami G (1996) J Electrochem Soc 143:1547–1550
18. Shiyanovskaya I, Hepel M (1999) J Electrochem Soc 146:243–249
19. Kamada K, Mukai M, Matsumoto Y (2002) Electrochim Acta 47:3309–3313
20. Pauporte Th, Goux A, Kahn-Harari A, Tacconi NR, Chenthamarakshan CR, Rajeshwar K, Lincot D (2003) J Phys Chem Solids 64:1737–1742
21. Tacconi NR, Chenthamarakshan CR, Rajeshwar K, Pauporte T, Lincot D (2003) Electrochem Comm 5:220–224
22. Tacconi NR, Chenthamarakshan CR, Wouters KL, MacDonnell FM, Rajeshwar K (2004) J Electroanal Chem 566:249–256
23. Somasundaram S, Tacconi N, Chenthamarakshan CR, Rajeshwar K, Tacconi NR (2005) J Electroanal Chem 577:167–177
24. Georgieva J, Armyanov S, Valova E, Tsacheva Ts, Poulios I, Sotiropoulos S (2005) J Electroanal Chem 585:35–43
25. Somasundaram S, Chenthamarakshan CR, Tacconi NR, Basit NA, Rajeshwar K (2006) Electrochem Commun 8(4):539–543
26. Georgieva J, Armyanov S, Valova E, Poulios I, Sotiropoulos S (2006) Electrochim Acta 51(10):2076–2087
27. Georgieva J, Armyanov S, Valova E, Poulios I, Sotiropoulos S (2007) Electrochem Commun 9:365–370
28. Georgieva J, Armyanov S, Valova E, Philippidis N, Poulios I, Sotiropoulos S (2008) J Adv Oxid Technol 11(2):300–307
29. Valova E, Georgieva J, Armyanov S, Sotiropoulos S, Hubin A, Baert K, Raes M (2010) J Electrochem Soc 157(5):D309–D315
30. Georgieva J, Sotiropoulos S, Armyanov S, Philippidis N, Poulios I (2011) J Appl Electrochem 41:173–181
31. Enea O (1996) Electrochim Acta 41:473–476
32. Nogueira AF, Longo C, De Paoli M (2004) Coord Chem Rev 248:1455–1468
33. Wang Y (2009) Sol Energy Mater Sol Cells 93:1167–1175
34. Ichikawa S, Doi R (1996) Catal Today 27:271–277
35. Seger B, Kamat PV (2009) J Phys Chem C 113:18946–18952
36. Georgieva J, Armyanov S, Poulios I, Sotiropoulos S (2009) Electrochem Comm 11(8):1643–1646
37. Georgieva J, Armyanov S, Poulios I, Jannakoudakis AD, Sotiropoulos S (2010) Electrochem Solid State Lett 13(10):P11–P13
38. Georgieva J, Sotiropoulos S, Armyanov S, Poulios I (2011) Int J Nanoparticles 4(2/3):216–230
39. Perry RH, Green DW, Maloney JO (eds) (1984) Perry's chemical engineer's handbook, 6th edn. McGraw-Hill, New York
40. Yamakata A, Ishibashi T, Onishi H (2003) J Phys Chem B 107:9820–9823
41. Montoya JF, Velasquez JA, Salvador P (2009) Appl Catal B 88:50–58
42. Georgieva J, Sotiropoulos S, Armyanov S, Valova E, Poulios I, Phillipides N (2009) In: Singh VG (ed) Applied electrochemistry: chemistry research and applications. Nova Science, New York, pp 301–334
43. Turchi CS, Ollis DF (1990) J Catal 122:178–192